

*promoting access to White Rose research papers*



**Universities of Leeds, Sheffield and York**  
**<http://eprints.whiterose.ac.uk/>**

---

This is an author produced version of a paper published in **Journal of Physics: Conference Series**.

White Rose Research Online URL for this paper:

<http://eprints.whiterose.ac.uk/77086/>

---

**Paper:**

Hardcastle, TP, Brydson, RMD, Seabourne, CR, Scott, AJ and Livi, KJT (2012) *Ab-initio modelling, polarity and energetics of clean rutile surfaces in vacuum and comparison with water environment*. In: Journal of Physics: Conference Series.

<http://dx.doi.org/10.1088/1742-6596/371/1/012059>

---

# Ab-initio modelling, polarity and energetics of clean rutile surfaces in vacuum and comparison with water environment

T.P. Hardcastle<sup>1</sup>, R.M.D. Brydson<sup>1</sup>, K.J.T. Livi<sup>2</sup>, C.R. Seabourne<sup>1</sup> and A.J. Scott<sup>1</sup>

1. Inst. for Materials Research, SPEME, University of Leeds, Leeds LS2 9JT, UK

2. HRAEM/IIC Facility, Johns Hopkins University, Baltimore, MD 21218 USA

penth@leeds.ac.uk

**Abstract.** All terminations of the (1x1) rutile (110), (101), (001), (100) and (111) surfaces are classified according to their electrostatic polarity. Six are found to be non-polar. The plane-wave density functional theory code CASTEP is used with a GGA-PBE exchange-correlation functional and a vacuum/material slab supercell method to calculate the surface energy density of symmetric thin rutile films with the six non-polar terminations in vacuum. The ratio of the surface energy densities of a rutile crystal with {111} and {110} facets in water is deduced using Lagrange multipliers and found to be consistent with the DFT vacuum results.

## 1. Introduction

The currently active research area of metal oxide surfaces has the curious and unusual attribute of producing fertile developments on a fundamental theoretical level by means of application of physics developed 150 years ago. Maxwell's theory of classical electrostatics was applied by Tasker in 1979 [1] to prototype model oxide surfaces providing a simple recipe for their classification on the basis of energetic stability. Subsequent developments regarding the polarity of oxide surfaces were elegantly summarised with classical arguments by Noguera in 2000 [2] and Goniakowski et al. in 2008 [3]. Alongside this, a modern quantum theory of dielectric polarisation emerged in the 1990's [4, 5, 6] in which polarisation is interpreted as a displacement of the centres of charge of Wannier functions. It is suggested [3] that the success of a classical approach based on point charges for insulating materials with highly localised orbitals is because Wannier functions can be mapped to a lattice of effective point charges as shown by Marzari and Vanderbilt in 1997 [7]. The merit of this suggestion is not investigated here, but the general success [8] of Tasker's system makes for convincing testimony.

In Goniakowski's 2008 paper, Maxwell's microscopic equations are assumed to apply at the surface of a uniform semi-infinite isotropic dielectric material. It is shown that such a material existing in the ground state cannot sustain a macroscopic polarisation in the absence of an external electric field:

$$\langle \bar{P}_x \rangle = \mu_B(x_s)/aS - \sigma_s(x_s) = 0, \quad (1)$$

where  $\langle \bar{P}_x \rangle$  is the laterally-averaged polarisation density of the surface cell in the surface-normal direction  $x$ ,  $\mu_B$  is the  $x$ -component of the electric dipole moment of the bulk cell,  $\sigma_s$  is the total charge in the surface cell divided by its surface area  $S$ ,  $a$  is the surface-normal lattice parameter of the bulk cell and  $x_s$  is the  $x$  coordinate of a Gibbs dividing surface (on which the bulk and surface cell definitions depend) chosen to denote the location of the boundary shared by the surface cell and the bulk cell directly below it. Equation (1) is useful since it can be interpreted as a stability condition. Its

violation implies non-zero polarisation and consequent instability of the termination in question. It is also independent of the chemical identity of the charge distribution, allowing for the stabilising (or otherwise) effect of charged adsorbates placed in the surface cell to be predicted. Furthermore, it is just a more general way of expressing Tasker's well-known surface instability condition,  $\mu_S \neq 0$ , where  $\mu_S$  is the surface cell dipole. By defining the bulk and surface cells identically using  $\mu_B \equiv \mu_S$ , we obtain  $\sigma_S = 0$  on account of bulk cell neutrality and hence recover  $\mu_S = 0$  for stability and  $\mu_S \neq 0$  for instability as expected. Tasker's classification does not depend on exact ionic charge allocations and applies *prior to cleaving* (Indeed, it can be used to *predict* surface reconstructions required to stabilise polar surfaces.) so a robust, canonical indication of stability can be obtained using frozen-bulk termination atomic positions and formal ionic point charge values in equation (1) by merely identifying  $\langle \bar{P}_x \rangle \neq 0$  as the necessary and sufficient condition for surface termination instability.

For Miller indices  $h, k, l = 0, 1$  there are 14 unique frozen bulk terminations of the rutile structure, having eliminated equivalent terminations by virtue of space group symmetries. Summing over atomic species labels  $j$  and same-species atom labels  $i$ , with  $\mu_B(x_S) = \sum_{\text{bulk cell}} q_i^j (x_i^j - x)$  and  $\sigma_S(x_S) = \frac{1}{S} \sum_{\text{surface cell}} q_i^j$  with formal charges  $q_i^{Ti} = +4$ ,  $q_i^O = -2$  and using bulk atomic positions, equation (1) can be used to classify these 14 terminations by polarity as shown in Table 1.

| Surface plane | Termination                             | $\langle \bar{P}_x \rangle / e\text{\AA}^{-1}$ | Surface plane | Termination  | $\langle \bar{P}_x \rangle / e\text{\AA}^{-1}$ |
|---------------|---|--|---------------|--|--|
| (111)         | TiO <sub>2</sub> /O/Ti/O/...            | 0  | (101)         | O <sub>2</sub> /Ti <sub>2</sub> /O <sub>2</sub> /... | 0  |
|               | O/Ti/O/TiO <sub>2</sub> /...            | 0  |               | Ti <sub>2</sub> /O <sub>2</sub> /O <sub>2</sub> /... | -0.16  |
|               | Ti/O/TiO <sub>2</sub> /O/...            | -0.07  |               | O <sub>2</sub> /O <sub>2</sub> /Ti <sub>2</sub> /... | 0.16   |
|               | O/TiO <sub>2</sub> /O/Ti/...            | 0.07   | (100)         | O/Ti/O/...   | 0  |
| (110)         | O/Ti <sub>2</sub> O <sub>2</sub> /O/... | 0  |               | Ti/O/O/...   | -0.15  |
|               | Ti <sub>2</sub> O <sub>2</sub> /O/O/... | -0.10  |               | O/O/Ti/...   | 0.15   |
|               | O/O/Ti <sub>2</sub> O <sub>2</sub> /... | 0.10   | (001)         | TiO <sub>2</sub> /...                                | 0  |

**Table 1.** The formal polarity of low-index rutile frozen bulk terminations in vacuum. The termination columns list the repeat sequence of atomic planes lying parallel to the surface, where the leftmost entry denotes the surface-terminating plane. 6 terminations have exactly zero (by inversion symmetry) polarisation. The remaining 8 are polar. All arithmetic used bulk atomic positions obtained via the ICSD. Precision errors were negligible.  $\langle \bar{P}_x \rangle \neq 0$  values are shown to 2 significant figures.

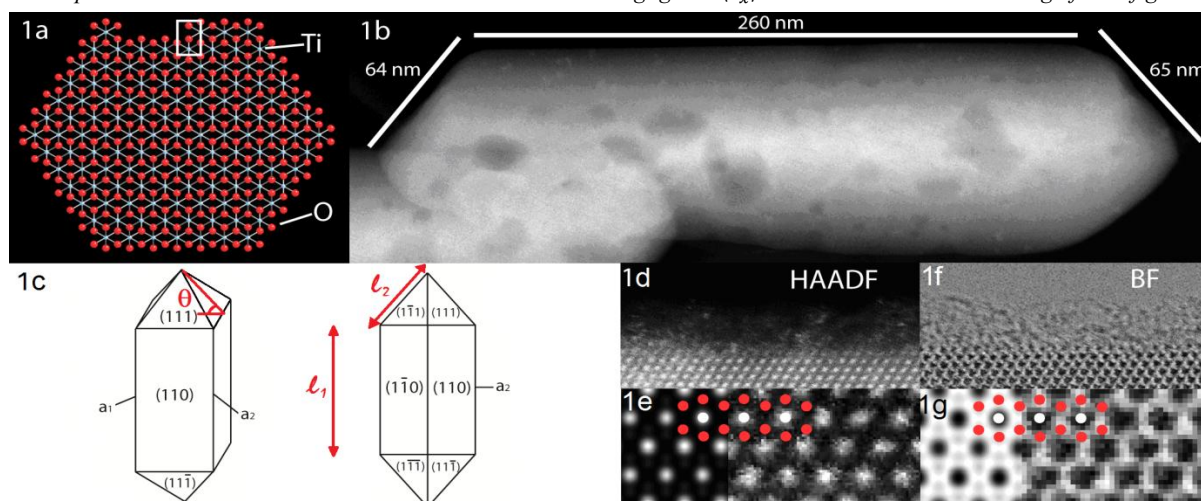


**Figure 1.** a) Model crystal viewed down  $[100]$  with steps at top. Steps currently being studied for abstract quoted at the end of this caption. Unit cell in white. b) A double-terminated crystal viewed down  $[100]$ . The length ratio of the  $\{110\}$  and  $\{111\}$  edges is 4:1. c) Crystal habit with edge lengths  $l_1, l_2$  and  $\theta = (90 - 47.67)^\circ = 42.33^\circ$ . d) Aberration-corrected HAADF image of  $\{110\}$  side viewed down  $[100]$  e) Simulated HAADF image with Ti atoms highlighted in white and O atoms in red. f) BF of  $\{110\}$  side viewed down  $[100]$  direction g) Simulated BF image with atoms highlighted as in 1e. Intensity at the edge in 1d and 1f is organic matter. **Images taken and adapted from abstract entitled "Imaging the surface of Rutile by STEM and its implication for organic molecule bonding" for MC2011 Conference Kiel, Germany, with permission of K. J. T. Livi.**

The vacuum polarity classification in Table 1 filters out polar surfaces, whose surface energies diverge [1], leaving the 6 non-polar surfaces for which convergent vacuum surface energy calculations can be carried out using the periodic supercell method, and comparisons drawn with crystals in non-vacuum environments. One current area of research ripe for such comparison is that of rutile surfaces

in an aqueous environment with organic adsorbates. Livi et al. used aberration-corrected STEM HAADF and BF imaging at SuperSTEM in Daresbury, UK, to study rutile crystals which crystallised with a square prism and double-terminated square pyramid habit with  $\{110\}$  and  $\{111\}$  facets, different from the well-known vacuum equilibrium habit [12], exposed to water and organic matter as shown in Fig. 1. Using an approach like that of Table 1 for the real surface in the presence of a non-trivial chemical environment would require a much more realistic approach to surface chemistry. The adsorption modes of the organic material can not be determined from the images owing to its amorphous appearance as seen in Fig. 1d and 1f. However, the surface energy density *ratio* of the aqueous-exposed crystal facets,  $\frac{\gamma_{111(\text{aqueous})}}{\gamma_{110(\text{aqueous})}}$ , can be inferred from the images, without specific knowledge of atomic-scale surface phenomena, by appealing to the Gibbs-Wulff theorem which states that a macroscopic crystal in equilibrium exists in a state of minimum total surface energy. An inverse Wulff construction can not be performed directly on Fig. 1b because of the  $[100]$  viewing direction; the crystal facets are not lying perpendicular to the plane of the page. Instead, elementary geometry can be applied to express the total crystal surface energy  $E_s$  and volume  $V$  in terms of the STEM-observed edge lengths  $l_1$  and  $l_2$ , and the (fixed) angle  $\theta$  as per Fig. 1c, to give the expressions  $E_s(l_1, l_2, \theta) = 8(1 + \sec^2\theta)^{-1/2}(l_1 l_2 \gamma_{110(\text{aqueous})} + l_2^2 \gamma_{111(\text{aqueous})} \sec\theta)$  and  $V(l_1, l_2, \theta) = 4(1 + \sec^2\theta)^{-1} \left( l_1 l_2^2 + \frac{2}{3}(1 + \sec^2\theta)^{-1/2} \tan\theta l_2^3 \right)$ . Then,  $E_s$  can then be minimised with respect to  $l_1$  and  $l_2$  whilst imposing the constraint  $V > 0$  by using the method of Lagrange multipliers, to relate the quantity  $\frac{\gamma_{111(\text{aqueous})}}{\gamma_{110(\text{aqueous})}}$  to the observables  $l_1$  and  $l_2$ . This method is just an algebraically explicit inverse Wulff construction and is entirely equivalent. The result is equation (2a). The  $l_1 = 4l_2$ ,  $\theta = 42.33^\circ$  case, pertaining to the crystal in Fig. 1b, is evaluated to 3 significant figures in equation (2b).

$$\frac{\gamma_{111(\text{aqueous})}}{\gamma_{110(\text{aqueous})}} = \frac{l_1}{l_2} \left( \frac{\sqrt{1 + \sec^2\theta}}{2\sec\theta} \right) + \frac{\tan\theta}{\sec\theta} \quad (2a) \qquad \left. \frac{\gamma_{111(\text{aqueous})}}{\gamma_{110(\text{aqueous})}} \right|_{\substack{l_1=4l_2 \\ \theta=42.33^\circ}} = 3.16 \quad (2b)$$

## 2. Method

The density functional theory code CASTEP [9] was used to calculate the geometry-optimised ground state enthalpy of symmetric (same termination on each side) thin rutile films of increasing thickness in vacuum with the 6 non-polar terminations of surfaces (110), (101), (001), (100) and (111). Supercells containing a slab of rutile material and a vacuum slab were used along with the GGA-PBE exchange-correlation functional picked on the basis of a bulk lattice parameter validation test. The vacuum thickness  $c_{vac}$ , kinetic energy cut off  $E_k$  and k-point spacings  $s^{i=1,2,3}$ , where  $i$  denotes correspondence to the reciprocal space axis  $b_i$ , were set at  $c_{vac} = 10\text{\AA}$ ,  $E_k = 400\text{ eV}$  and  $s^{i=1,2,3} < 0.055\text{\AA}^{-1}$  for  $i = 1, 2, 3$ , based on numerical convergence tests. Slabs were constructed by stacking single unit cells with a starting thickness of 1  $\text{Ti}_2\text{O}_4$  unit cell for the (110), (101), (001), (100) films and 1.5  $\text{Ti}_2\text{O}_4$  unit cells for the two (111) films. Distinct calculations for each slab were performed up to a thickness of  $\sim 20\text{\AA}$ . All atoms in the slabs were allowed to relax, with the exception of atoms located further than  $8\text{\AA}$  in the surface normal direction from both surfaces for slabs of total thickness  $> 16\text{\AA}$ . The positions of these atoms were fixed to reduce computational cost. The surface energy density  $\gamma$  in each case was calculated using the ground state enthalpy output values  $E_{Ti_nO_{2n}}$  of the slab/vacuum supercells of formula  $Ti_nO_{2n}$  and total surface area  $2S$ , and a  $Ti_2O_4$  bulk cell enthalpy:

$$\gamma = 1/2S (E_{Ti_nO_{2n}(\text{supercell})} - n/2 E_{Ti_2O_4(\text{bulk})}) \quad (3)$$

## 3. Results and Discussion

The CASTEP output is shown in Fig. 2. The plots were extrapolated with a 4-point weighted mean to give the  $\gamma$  values in Table 2. No absolute measurements of termination-specific rutile surface energies yet exist, but these results are consistent with previous ab-initio studies of rutile surfaces in vacuum [10, 11, 12]. The (111)(O) slabs underwent relaxations with a non-trivial relationship with thickness. Slab energy convergence behaviour appears to have been investigated only for the (110) surface [13].

| Non-polar termination type                           | (110)           | (100)           | (101)           | (001)           | (111)(TiO <sub>2</sub> ) | (111)(O)        |
|--|-----------------|-----------------|-----------------|-----------------|--------------------------|-----------------|
| $\gamma_{(termination\ type)(vac)} / \text{Jm}^{-2}$ | $0.42 \pm 0.08$ | $0.62 \pm 0.08$ | $0.98 \pm 0.08$ | $1.15 \pm 0.08$ | $1.33 \pm 0.08$          | $1.35 \pm 0.08$ |

**Table 2.** CASTEP results for  $\gamma$  in vacuum to 2 significant figures. Precision errors from basis set and extrapolation errors.

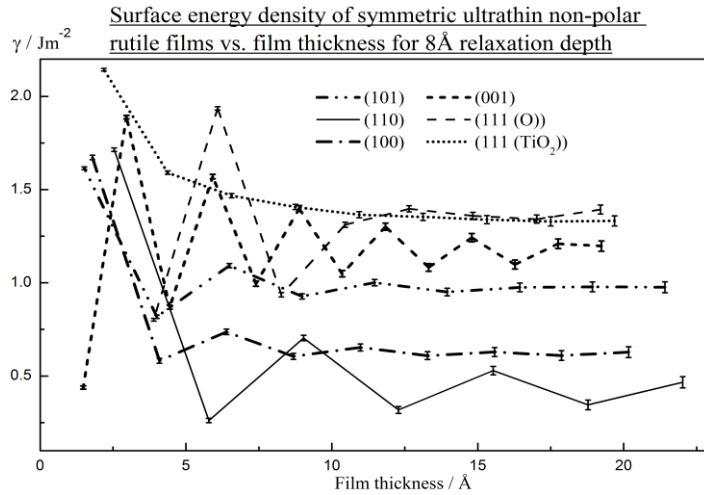


**Figure 2.** Symmetric non-polar ultrathin film surface behaviour converging to that of semi-infinite surfaces in vacuum with increasing thickness. Termination type indicated in brackets for (111) plots.

The importance of surface chemistry on crystal growth has been demonstrated elsewhere [14]. The CASTEP results obtained in this paper for clean surfaces in vacuum should be regarded as a basis for comparison with non-vacuum environments. The crystalline rutile studied by Livi et al., the example studied here, in the water/organic environment shown in Fig. 1b shows a length ratio of 4:1 for the water/organic-exposed {110} and {111} facet edge lengths  $l_1$  and  $l_2$ , corresponding to a surface energy density ratio  $\frac{\gamma_{111(aqueous)}}{\gamma_{110(aqueous)}} = 3.16$  as shown in equation (2b). In order to gain some insight into the significance of the aqueous/organic environment on the relative surface energy densities of the (111) and (110) surfaces this ratio can be compared to the vacuum case by using the CASTEP values from Table 2 to evaluate the two ratios  $\frac{\gamma_{(111(TiO_2))(vac)}}{\gamma_{(110)(vac)}}$  and  $\frac{\gamma_{(111(O))(vac)}}{\gamma_{(110)(vac)}}$ . These values, calculated to 3 significant figures, are shown in equations (4a) and (4b). The precision errors arise primarily from the extrapolation method used.

$$\frac{\gamma_{(111(TiO_2))(vac)}}{\gamma_{(110)(vac)}} = 3.17 \pm 0.63 \quad (4a)$$

$$\frac{\gamma_{(111(O))(vac)}}{\gamma_{(110)(vac)}} = 3.21 \pm 0.64 \quad (4b)$$

It can be seen that  $\frac{\gamma_{(111(TiO_2))(vac)}}{\gamma_{(110)(vac)}} \approx \frac{\gamma_{(111(O))(vac)}}{\gamma_{(110)(vac)}} \approx \frac{\gamma_{111(aqueous)}}{\gamma_{110(aqueous)}}$ , suggesting that *the aqueous environment has no significant effect on the relative surface energy densities of the (110) and (111) surfaces*. This result predicts nothing about absolute changes in the (110) and (111) surface energies.

#### 4. Conclusions

The surface energy densities of the rutile (111)(O) and (111)(TiO<sub>2</sub>) surfaces in vacuum were predicted for the first time at  $1.35 \pm 0.08 \text{ Jm}^{-2}$  and  $1.33 \pm 0.08 \text{ Jm}^{-2}$  respectively. The surface energy density ratio of (110) and (111) rutile surfaces in vacuum does not differ significantly in an aqueous environment.

#### 5. References

- [1] Tasker P 1979 *Journal of Physics C Solid State Physics* **12** 4977
- [2] Noguera C 2000 *Journal of Physics: Condensed Matter* **12** R367
- [3] Goniakowski J et al. 2008 *Reports on Progress in Physics* **71** 016501
- [4] Vanderbilt D 1993 *Physical Review B*. **48** 4442–4455
- [5] King-Smith R and Vanderbilt D 1993 *Physical Review B*. **47** 1651–1654
- [6] Resta R 1994 *Reviews of Modern Physics* **66** 899–915
- [7] Marzari N and Vanderbilt D 1997 *Physical Review B*. **56** 12847–12865
- [8] Diebold U 2003 *Surf. Sci. Reports* **48** 53–229
- [9] Clark S J et al. 2005 *Zeitschrift fuer Kristallographie* **220** 567–570
- [10] Perron H et al. 2007 *Theor. Chem. Acc.* **117** 565–574
- [11] Kiejna A et al. 2006 *Journal of Physics: Condensed Matter* **18** 4207–4217
- [12] Ramamoorthy M and Vanderbilt D 1994 *Physical Review B*. **49** 16721–16727
- [13] Bredow T et al. 2004 *Physical Review B*. **70** 035419
- [14] Barnard A S and Curtiss L A 2005 *Nano Letters* **5** 1261–1266